



Published in final edited form as:

Neuroinformatics. 2005 ; 3(3): 263–280. doi:10.1385/NI:3:3:263.

Effects of Random External Background Stimulation on Network Synaptic Stability After Tetanization:

A Modeling Study

Zenas C. Chao¹, Douglas J. Bakkum¹, Daniel A. Wagenaar², and Steve M. Potter^{*,1}

¹Department of Biomedical Engineering, Georgia Institute of Technology, Atlanta, GA 30332-0535, USA

²Department of Physics, California Institute of Technology, Pasadena, CA 91125, USA

Abstract

We constructed a simulated spiking neural network model to investigate the effects of random background stimulation on the dynamics of network activity patterns and tetanus induced network plasticity. The simulated model was a “leaky integrate-and-fire” (LIF) neural model with spike-timing-dependent plasticity (STDP) and frequency-dependent synaptic depression. Spontaneous and evoked activity patterns were compared with those of living neuronal networks cultured on multi-electrode arrays. To help visualize activity patterns and plasticity in our simulated model, we introduced new population measures called Center of Activity (CA) and Center of Weights (CW) to describe the spatio-temporal dynamics of network-wide firing activity and network-wide synaptic strength, respectively. Without random background stimulation, the network synaptic weights were unstable and often drifted after tetanization. In contrast, with random background stimulation, the network synaptic weights remained close to their values immediately after tetanization. The simulation suggests that the effects of tetanization on network synaptic weights were difficult to control because of ongoing synchronized spontaneous bursts of action potentials, or “barrages.” Random background stimulation helped maintain network synaptic stability after tetanization by reducing the number and thus the influence of spontaneous barrages. We used our simulated network to model the interaction between ongoing neural activity, external stimulation and plasticity, and to guide our choice of sensory-motor mappings for adaptive behavior in hybrid neural-robotic systems or “hybrots.”

Index Entries

Cultured neural network; spike-timing-dependent plasticity (STDP); frequency-dependent depression; multi-electrode array (MEA); spatio-temporal dynamics; tetanization; model; plasticity; cortex; bursting; population coding

Introduction

In vitro model systems are helpful to understand brain functions because they reduce the brain's overwhelming complexity. For example, cultured networks have been used to study the nervous system because the external inputs are well controlled and do not compete with the behavioral drives of an intact animal, such as thirst and attention. Added advantages include high accessibility to microscopic imaging and pharmacological manipulation. Cultured networks express many aspects of the neural dynamics observed in animals while providing a

*Author to whom all correspondence and reprint requests should be addressed. E-mail: steve.potter@bme.gatech.edu.

much simpler network to study. By applying multi-electrode array (MEA) technology, researchers have recorded and electrically stimulated cultured networks at multiple spatial locations (Gross et al., 1993b; Tateno and Jimbo, 1999; Shahaf and Marom, 2001). We developed a closed-loop paradigm (Potter et al., 1997; DeMarse et al., 2001; Potter et al., 2004) consisting of a sensory-motor loop between a cultured network and a robot or animat (Meyer and Wilson, 1991) in order to study sensory processing, memory formation, and behavioral control. We call this embodied hybrid neural-robotic system a “hybrot” (Fig. 1) (Potter et al., 2004).

Left to themselves in culture medium, dissociated neurons spontaneously grow and form synapses with neighboring neurons, developing complex patterns of activity that suggest an intrinsic drive to form a network and share information. Little is understood of this activity or how its plasticity relates to adaptive behavior in animals. By embodying an in vitro model in an environment with chosen physical associations, we hope to discover how it could learn these associations. We have used cultures on MEAs in several hybrot (Bakkum et al., 2004) for studying sensory-motor dynamics in cultured networks, but in order to study learning behavior, we need a better understanding of plasticity at the network level. Here we applied a neural network simulation approach to investigate the interactions between ongoing network activity, external stimulation, and network plasticity to better choose the mappings from neural activity to hybrot behavior and from environmental feedback to neural stimulation.

Activity-dependent modification of synaptic strength plays a central role in the learning and memory processes in the central nervous system (Bliss and Collingridge, 1993). Two important cellular mechanisms of synaptic modification, long-term potentiation (LTP) (Bliss and Lomo, 1973) and long-term depression (LTD) (Linden, 1994), have been studied mainly as changes in the response of single neurons or in local field potentials at single sites. Those changes in response have been experimentally induced by a strong electrical stimulation called a tetanus. Jimbo and co-workers have shown that these cellular plasticity mechanisms scale to the network level, studied in cultured neurons on MEAs (Jimbo et al., 1999). In their study both LTP and LTD were observed, though the change could not be predicted or controlled. This lack of predictability and controllability makes it difficult to create effective learning protocols for hybrot. We hypothesize that the effects of a tetanus on network synaptic weights are difficult to control because the synaptic weights are driven to other attractors by the synchronized spontaneous bursts of action potentials, or “barrages,” which are the most prominent feature of the electrical activity of dissociated cortical cultures (Gross et al., 1993a; Wong et al., 1993; Kamioka et al., 1996; Gross and Kowalski, 1999). Our simulation compared the relative contributions of ongoing spontaneous activity and input tetanization on network plasticity.

Methods

Living Cultured Neuronal Network Model

Cell Culture, Recording, and Stimulation System—Dense cultures of dissociated neocortical neurons were prepared as described before (Potter and DeMarse, 2001). Briefly, embryonic rat cortices were dissected and dissociated using papain and trituration. Cells were densely plated (2500 cells/mm²) on MEAs (MEAs; MultiChannel Systems, Reutlingen, Germany) precoated with polyethyleneimine and laminin. Cultures were allowed to mature for 3 wk in serum-containing Dulbecco's Modified Eagle Medium (DMEM)-based medium before experiments were performed. Stimuli (biphasic, 600 mV × 400 μs) were delivered using our custom-made stimulator (Wagenaar and Potter, 2004). Responses were recorded using MultiChannel Systems hardware and our publicly available acquisition and analysis software, Meabench.¹

Stimulation Protocol—Random background stimulation was performed on one cultured network. For all 53 usable electrodes, 53 trains of 1/53 Hz stimulation generated by a Poisson process were applied.

Artificial Neural Network Model

The Neural Circuit Simulator (Natschlagler et al., 2002) was modified to produce five artificial neural networks with the following features. 1000 leaky integrate-and-fire (LIF) neurons with a total of 50,000 synapses were placed randomly in a 3 mm × 3 mm area (*see* Fig. 2A). All synapses were frequency-dependent (Markram et al., 1998; Izhikevich et al., 2004) to model synaptic depression; the synaptic efficacy was determined by the probability of release of neurotransmitters depending on the mechanism of frequency dependence, which recovered with a time constant of 12 ms. Seventy percent of the neurons were excitatory, with STDP (Song et al., 2000) at all excitatory synapses. The other neurons were inhibitory (30%) (Marom and Shahaf, 2002). The distribution of the synaptic connection distances followed the distribution found by Segev and Ben-Jacob (Segev and Ben-Jacob, 2000): neurons tend to make many short synaptic connections but a few long ones as well. The number of synaptic connections per neuron followed a Gaussian distribution and each neuron had 50 ± 33 synapses onto other neurons. The conduction delay was proportional to the synaptic connection distance, and the conduction velocity was set to be 0.3 m/s (Kawaguchi and Fukunishi, 1998). Gaussian random noise was introduced into each neuron independently as fluctuations in membrane voltage: 30% of the neurons (“self-firing neurons”) had variance at a high enough level to initiate spikes (Latham et al., 2000), whereas the rest exhibited only subthreshold fluctuations. An 8 × 8 grid of electrodes with 333 μm inter-electrode spacing was included. All electrodes could be used for stimulation, and 60 of these (except corner electrodes 11, 18, 81, and 88) were used for recording (Fig. 2B). One stimulation electrode stimulated 76 ± 12 ($n = 5$ simulated networks) of the closest neurons.

Some differences between our artificial neural network and our living network should be noted. In our artificial neural network, external stimulation was set to generate activity only on nearby neurons’ “cell bodies;” an electrode affected about 76 neurons. However, electrical stimulation applied to our cultured neurons by an MEA could also evoke action potentials on axons (McIntyre and Grill, 2002; Wagenaar et al., 2004), generating spikes on neurons that may be far from the electrode, directly without synaptic transmission. Unfortunately, little experimental evidence exists for the number of neurons or the range that one stimulus electrode could affect in cultured living networks.

Artificial Neural Network Initialization and Stimulation Protocol

All excitatory synaptic weights were initially set to 0.05 and could vary between zero and 0.1 owing to STDP. At the maximal weight, each spike would have a 50% probability of evoking a spike in postsynaptic neuron, owing to its summation with intrinsic noise. The synaptic weights for the inhibitory connections were fixed at -0.05 . The networks were run for 2 h in simulated time until the synaptic weights reached the steady state. Most of the excitatory synaptic weights ($93 \pm 2\%$) in five simulated networks were less than 0.01 or greater than 0.09. This bimodal steady-state distribution of weights arose from the STDP learning rule, as previously observed by Song et al. (2000), and Izhikevich and Desai (2003). The set of synaptic weights after 2h, which stabilized without external stimuli, was used for the subsequent simulation experiments as the initial state. Some of the parameters in our simulated network were approximated from studies of acute slices (Markram et al., 1998; Song et al., 2000) and from the simulation of neocortical networks (Izhikevich et al., 2004).

¹<http://www.its.caltech.edu/~wagenaar>

Two types of electrical stimuli were delivered to the simulated networks, *tetanzation* and *background* stimuli. Tetanzation was applied simultaneously at two stimulation electrodes (electrode 33 and 66, *see* Fig. 2B) at 20 Hz for either 10 s or 5 min; tetanzation was used to induce change in the network synaptic weights. The background stimuli were applied to all 64 electrodes, one at a time, with random intervals generated by Poisson process, at an average rate of 1/64 Hz per electrode. Thus, each electrode stimulated the simulated network with different random sequences, at an average of one pulse per second for the whole array.

Four experiments were performed on each of five simulated networks to investigate how the tetanzation and the random multisite background stimulation affected the network synaptic weights:

“Short”: Spontaneous activity was recorded for 10 min (pretetanzation period), before a short tetanzation was applied for 10 s. After tetanzation, spontaneous activity was recorded for an additional 50 min (posttetanzation period).

“Long”: Same as “Short,” but the tetanzation period was 5 min instead of 10 s.

“Short+Background”: Same as “Short,” but with random multisite background stimulation turned on during the whole simulation.

“Long+Background”: Same as “Long,” but with random multisite background stimulation turned on during the whole simulation.

Measures of Network Activity and Network Synaptic Weights

To help visualize activity patterns and plasticity in the artificial neural network, we introduce the Center of Activity (CA) and Center of Weight (CW) (analogous to center of gravity) to describe the spatio-temporal dynamics of the network-wide firing activity and network-wide synaptic strength in our simulated networks, respectively.

Calculation of CA—The spatio-temporal patterns of network-wide population activity is described by CA trajectories in this study. The CA indicates the magnitude of total activities and the “inhomogeneity” of the spatial activity distribution. That is, if the network is firing “homogeneously” the CA will be at the center of the dish, whereas if the network fires mainly in one corner then the CA will move to that direction.

Assume A is a 1 by 1000 vector which represents the number of spikes at 1000 neurons in the interval $[t, t+TW]$, where TW is a small time window. To maintain a sufficient amount of spikes and high temporal resolution, TW was chosen as 10 times the integration time step of simulation. Let $X(i)$ and $Y(i)$ indicate the horizontal and vertical distances from the i th neuron to the center of the 3 mm \times 3 mm dish, respectively. Then the CA at time t is a two dimensional vector

$$\vec{CA}(t) = \frac{\sum_{i=1}^{1000} A(i) \cdot [X(i), Y(i)]}{\sum_{i=1}^{1000} A(i)} \quad (1)$$

The CA trajectory from time t_0 to t_1 with time step Δt (set to 1/5 th of TW) is defined as

$$\overrightarrow{\text{trajectory}}(t_0, t_1) = [\vec{CA}(t_0), \vec{CA}(t_0 + \Delta t), \vec{CA}(t_0 + 2\Delta t), \dots, \vec{CA}(t_1)] \quad (2)$$

The CA is related to the population vector description (Caminiti et al., 1990), in that both are vector summations of activity, but it is distinct. The population coding principle seems to be widespread in the brain, since it has been found in the motor cortex (Georgopoulos, 1994), premotor cortex (Caminiti et al., 1990) and other cortical areas. It demonstrates how the firing rates of a group of broadly tuned (e.g., to a direction of arm movement) neurons taken together provide an accurately tuned representation. Instead, the CA depicts the “population activity flow” in the neuronal circuitry space on a much quicker time scale.

Spontaneous Barrage Detection and Clustering of Barrage CA Trajectories—

Spontaneous barrages in simulated networks were classified into different clusters according to their CA trajectories. A firing rate histogram was obtained by counting the number of spikes network-wide in 10 ms bins. Bins with more than 20 spikes were considered a part of a barrage. The length of the barrage was defined as the time span of consecutive bins with a number of spikes over this threshold. CA trajectories were calculated for each barrage and aligned to each other at the peaks of the corresponding firing rate histograms. This alignment had similar results but operated more efficiently compared with shifting the lag on one trajectory to gain the highest cross-correlation with another. The beginnings and/or the ends of the CA trajectories of shorter than maximum length were padded with zeros. Each same-length CA trajectory was then reshaped into a one-dimensional vector by appending the y values of its CA trajectory to the x values. Clustering was performed with the k -means algorithm, run multiple times for different k values. The best of the clustering results was selected by choosing the k value with best Davies–Bouldin validity index (Davies and Bouldin, 1979).

Calculation of CW—Plastic changes in the simulated networks' functional architecture can be represented by the trajectory of the CW. Let W be a 1 by N vector, where N is the total number of excitatory synapses, representing the weights of every synapse at time t . Let $X(i)$ and $Y(i)$ indicate the horizontal and vertical distances from the postsynaptic neuron of the i th synapse to the center of the dish. Then, the CW of time t is a two dimensional vector

$$\vec{CW}(t) = \frac{\sum_{i=1}^N W(i) \cdot [X(i), Y(i)]}{\sum_{i=1}^N W(i)} \quad (3)$$

The CW trajectory from time t_0 to t_1 with time step Δt is defined as

$$\overrightarrow{\text{trajectory}}(t_0, t_1) = [\vec{CW}(t_0), \vec{CW}(t_0 + \Delta t), \vec{CW}(t_0 + 2\Delta t), \dots, \vec{CW}(t_1)] \quad (4)$$

Note that while the CA trajectory describes the spatio-temporal patterns of signal propagation in typically brief time intervals, the CW trajectory shows the dynamics of connection strengths changing over a typically larger time scale. In our case, the CA represented the neural activity flowing during a barrage whereas the CW described the network's plasticity over the duration of a simulation.

Results

We first compared our simulated neural network with living networks of rodent cortical neurons. Our LIF model and the living networks expressed similar spontaneous activity patterns. Raster plots and firing rate histograms of spontaneous activity and evoked responses obtained from both in vitro and simulated networks are shown together for comparison and a remarkable similarity was achieved (Fig. 3). For spontaneous activity, the barrage rates were

0.70 Hz and 0.73 Hz, and the proportion of spikes in barrages were 76% and 71%, in living and simulated networks, respectively (Fig. 3A,B).

In order to investigate the effects of tetanization on patterns of spontaneous activity, the CA trajectories were calculated for every spontaneous barrage in the artificial neural networks. Figures 4 and 5 depict 2387 barrages detected in the “long” experiment. The CA trajectories of these barrages were calculated and classified by the *k*-means clustering algorithm (*see* Methods), and 11 clusters were found (Fig. 4A).

The simulated network's spontaneous activity was changed by tetanization (Fig. 4B). Some types of barrages happened mostly in the 10-min pretetanization period, such as clusters 5, 9, and 11, whereas different barrages happened in the posttetanization period, such as clusters 1, 3, 7, 8, and 10. Most of the clustered barrages ceased to occur for some minutes after tetanization and reappeared later. For example, cluster 2 reappeared around $t = 25$ min, sooner than cluster 4, which reappeared around $t = 40$ min. Some clusters were transient, such as cluster 1 being highly concentrated around $t = 30$ min.

We studied the changes in synaptic weights that might underlie the differences in spontaneous barraging activity before and after tetanization. The CW trajectory of the simulated synaptic weights, shown in the “Long” experiment in Fig. 5B, was calculated and sampled at 2 Hz over the entire 67 min simulation. The trajectory was divided into four periods (Fig. 4B).

Pretetanization

(*P*): from $t = 0$ min to $t = 10$ min, the CW trajectory remained within a localized area we termed a “steady state.”

Tetanization

(*T*): from $t = 10$ min to $t = 15$ min, the CW was driven away from the steady state of period *P*. No spontaneous barrages occurred during this period.

Posttetanization drifting

(*D*): from $t = 15$ min to $t = 60$ min, after the tetanization, the CW drifted for about 45 min without external stimulation. As shown in Fig. 4B, different types of spontaneous barrages gradually appeared and disappeared during this period.

Posttetanization steady-state

(*S*): after $t = 60$ min, the CW arrived at a new steady state where it remained.

We compared the effects of 10 s and 5 min tetanizations by investigating the CW trajectories between the “Short” and the “Long” experiments (Fig. 5A,B), and the “Short+Background” and the “Long+Background” experiments (Fig. 5C,D). All drove the CW away from the pretetanization steady state. The CW distance between the centroid of the pretetanization steady state and the tetanization end point was used to quantify the effects of tetanization in changing network synaptic weights. This distance and standard error of the mean (SEM) ($n = 5$ simulated networks) was $79.5 \pm 6.0 \mu\text{m}$ in the “Long” experiments, significantly greater than $28.9 \pm 2.5 \mu\text{m}$ in the “Short” experiments ($p < 10^{-4}$, two-tailed *t*-test); and was $75.7 \pm 5.2 \mu\text{m}$ in the “Long+Background” experiments, significantly greater than $32.8 \pm 2.8 \mu\text{m}$ in the “Short+Background” experiments ($p < 10^{-4}$) (Fig. 6A).

In previous studies to model the restoration of sensory input to our living in vitro networks, we applied multisite background stimulation. This decreased or eliminated the occurrence of spontaneous barrages (Madhavan et al., 2003; Wagenaar et al., 2003, 2005). Here, using our

simulated networks, we investigated the influences of simulated random multisite background stimulation on the short and long tetanizations by quantifying the differences in CW trajectories with or without random low-frequency 64-electrode stimulation (averaging 1 Hz) (Fig. 5). With background stimulation, the CW did not move back to the pretetanzation steady state even after only 10 s of tetanization, unlike without background (Fig. 5C). The CW distance between the centroids of pre- and posttetanzation steady states was used to quantify the difference between the “Short” and the “Short+Background.” The distance was $7.17 \pm 1.01 \mu\text{m}$ ($n = 5$ simulated networks) in the “Short” experiments, much shorter than $56.2 \pm 10.5 \mu\text{m}$ in the “Short+Background” experiments ($p < 0.001$) (Fig. 6B).

In addition to preventing “turning-back” of the CW after a 10 s tetanization, background stimulation also reduced “drifting-away” of the CW after a 5 min tetanization. CW trajectories of a “Long” and “Long+Background” experiment from the same network are shown in Fig. 5. With random multisite background stimulation, the CW stayed near its value immediately after tetanization (Fig. 5D). Without random multisite background stimulation, the CW drifted and came to rest at a new steady state (Fig. 5B). The CW distance between the centroid of the posttetanzation steady state and the turn-off point of the tetanization was used to quantify the drifting of the CW after the tetanization. This distance was $77.6 \pm 15.2 \mu\text{m}$ ($n = 5$ simulated networks) in the “Long” experiments, much longer than $24.0 \pm 7.1 \mu\text{m}$ in the “Long+Background” experiments ($p < 0.01$) (Fig. 6B).

Although, background stimulation stabilized the network against large CW drift, small CW variations in the pre- and posttetanzation steady states were higher with the background stimulation than those without background stimulation (Fig. 5). The mean distance of individual CWs in the pretetanzation steady state from their centroids was used to quantify the spread of the CW. The spread was $2.9 \pm 0.2 \mu\text{m}$ ($n = 5$ simulated networks) without background stimulation, smaller than $9.8 \pm 0.8 \mu\text{m}$ with background stimulation ($p < 10^{-4}$). This spread was compared with the change of CW caused by tetanization, which was quantified by the CW distance between the centroid of the pretetanzation steady state and the tetanization end point. Without background stimulation, the spread was significantly smaller than the short tetanization-induced change ($p < 10^{-6}$) and significantly smaller than long tetanization-induced change ($p < 10^{-6}$). With background stimulation, the spread was significantly smaller than the short tetanization-induced change ($p < 10^{-4}$) and also significantly smaller than long tetanization-induced change ($p < 10^{-5}$) (Fig. 6A).

Discussion

Effects of Random Multisite Background Stimulation in Simulated and Living Networks

Random background stimulation helped maintain the stability of network synaptic weights after tetanization in simulated networks. The CW plots (Fig. 5) showed that the network synaptic weights tend toward a localized set of values, and that tetanization moves the network synaptic weights away. In the absence of background stimulation, the CW returned to its previous locus after a short tetanization, suggesting this locus served as an attractor. After a long tetanization, the CW drifted for some time before settling on a new attractor, suggesting the tetanization effect is not stable. With background stimulation, a short tetanization *can* change the network synaptic weights (Figs. 5 and 6); to use a mechanical analogy, the ‘elastic’ change becomes a ‘plastic’ change. A long tetanization will drive the network to a new locus, where it remains without drifting. The observation of CW attractors suggests that a form of self-organization or homeostasis exists in the interaction of synaptic weights and network activity; however, much remains to be studied about the mechanisms of this interplay.

We hypothesized that the network synaptic weights drifted after a tetanization because of the ongoing spontaneous activity, consisting of mostly spontaneous barrages (Fig. 4B).

Spontaneous activity and network synaptic weights interacted with each other until reaching a stationary set of patterns in CA space and an attractor in CW space. With random background stimulation, spontaneous activity was reduced, and so the network synaptic weights were mainly affected by stimulus-evoked activity. Since background stimulation, and consequently the evoked activity, was random spatially and temporally, these stimuli had an unbiased randomizing effect on changing network synaptic weights. Thus, the size of CW attractors was greater with the background stimulation than without it (Figs. 5 and 6). In summary, whereas the background stimulation stabilized the network synaptic weights by preventing the directional drift caused by influences of transient spontaneous barrages after tetanization, the randomizing effect also increased the variation of network synaptic weights isotropically.

In both simulated networks and living cultured networks, spontaneous barrages were reduced by random background stimulation and stimulus-evoked activity became dominant. Random multisite background stimulation was applied to living neural networks also, and neural activity was recorded and compared with that of the simulated neural network (Fig. 7). In a typical 1-min recording, the ratio of the number of evoked barrages vs spontaneous barrages was 41 : 1 in the living network compared with 42 : 3 in the simulated network. Moreover, the spontaneous barrage rate was reduced from 0.70 Hz (Fig. 3A) to 0.017 Hz (1 barrage in 1 min) in the living network and was reduced from 0.73 Hz (Fig. 3B) to 0.05 Hz (3 barrages in 1 min) in the simulated network.

Stability in Other Systems

Long-term stability of spontaneous activity patterns was found in cortical slice cultures (Beggs and Plenz, 2004; Ikegaya et al., 2004), suggesting these recurrent patterns could be used by cortical circuits to store information for memories. Our simulation results support this hypothesis by showing that for an attractor in CW space, a finite set of clustered CA trajectories recurs. The results also show that tetanizations changed the network to different attractors, and random background stimulation eliminated CW drift after a tetanization. This suggests the tetanization altered the contents of the memory stored in the network, and that the random background stimulation reduced spontaneous transients, allowing a greater control over network plasticity. Preliminary results of tetanization on living networks support this view (Madhavan et al., 2005).

Control of Network Synaptic Weights and Implementation in Hybrot

The use of MEAs in hybrot provides a model system to simultaneously study behavior and detailed neuronal function, including plasticity underlying adaptation or learning. In our experiments, tetanus was used to induce plasticity. By adding background stimulation, the plasticity remained while the stability needed for memory was provided.

We created motor mappings to control the behavior of a robot based on the activity in a real neuronal network, and sensory mappings to stimulate the network based on the sensory input from a hybrot (Bakkum et al., 2004). The first step to demonstrate learning behavior, begun in this simulated modeling study, is to search for the relationship between the network synaptic weights and the network spatio-temporal activity patterns. We demonstrated that tetanization drives the network from one attractor to another. This is promising for hybrot, because if we can induce the network synaptic weights to change, we can show the behavior of a robot changing from one mode to another mode to demonstrate adaptive learning.

A potential mapping for hybrot control is to use the CA trajectory of the responses to the random background stimulation as motor commands (Fig. 8). Different forms of tetanization have different effects on network synaptic weights (such as long vs short tetanization, Figs. 5 and 6) and can serve as the feedback to a living network representing different sensory inputs. In

this case, network synaptic weights change during each tetanization and the changes are stabilized by continuous random background stimulation. Therefore, the behavior pattern of the hybrot would change after each sensory feedback and remain steady until the next feedback. In this study, we used the CW trajectories and the occurrence of spontaneous barrages with different CA trajectories to illustrate network plasticity in model networks. However, these two quantities cannot be easily applied in living networks. First, the synaptic weights of a living culture are not directly measurable by the extracellular electrodes of our MEAs. Second, background stimulation reduces the frequency of spontaneous barrages in living networks; thus, not enough spontaneous barrages occur to reliably cluster their CA trajectories or to provide instant reaction for generating motor commands. Thus, we expect the responses to background stimuli to be the better parameter for hybrot control.

CA and CW Trajectories

Finding structure in the complexity of multiple time-varying neural signals is difficult and likely requires the creation of new mathematical tools (Pesaran et al., 2002; Baruchi and Ben-Jacob, 2004; Beggs and Plenz, 2004; Brown et al., 2004). The CA and the CW were designed to map multiple spatio-temporal signals into a more comprehensible form whereas retaining enough detail to discriminate network states. The CA and CW trajectories give summary statistics about the network-wide properties as opposed to statistics on individual neurons. Note that the shapes of the trajectories are independent of the selection of the trajectory origin or of the spatial center of the network since they are linear summations of neural locations.

Most current methods for neural spike train data analysis, such as the cross-correlogram, cross intensity function, and joint peri-stimulus time histogram, yield information only about associations between pairs of neurons (Brown et al., 2004). To give information on the whole network, these methods would require large computational power to go through every possible pair of neurons and require further statistics to compare more than two recordings. Although, a CA trajectory cannot provide detailed information about individual neurons, it has the advantage of depicting the spatio-temporal dynamics of the whole network.

Conclusion

Using artificial neural networks to control robots is an active area of research and, in addition to directing studies in living neural networks, holds the potential for many promising products (Brooks, 1999; Krichmar and Edelman, 2002; Schaal et al., 2004). Most work in AI and robotic systems faces limitations in the ability to adapt to novel situations in real-time. By contrast, it is clear that biological neural systems excel at this. Much can be learned from the activity, morphology, and connectivity of biological neural networks to inform the design of future artificial networks. If future research on living networks, demonstrate that directed functional changes can be obtained by stimulating the network, then we expect to find corresponding morphological changes. Imaging neuronal networks using time-lapse multiphoton microscopy (Potter, 2005; Potter et al., 2001) is compatible with many-neuron electrophysiology. We are building a dedicated 2-photon/MEA microscope (Rambani et al., 2005). The “brain” of the hybrot system, unlike an animal's brain, holds still during behavior, and can be imaged in its entirety (Bakkum et al., 2004).

We have only begun to explore the effects of multisite background stimulation on networks (Wagenaar et al., 2005). We are applying a synergy of modeling simple networks, and multiunit experimentation on substantially more complex living ones. Simulated network studies help suggest new experiments for studying learning in vitro, while the experimentation helps us come up with better-simulated models for the network-level properties of neural circuits. By embodying in vitro networks with hybrots in closed-loop systems, we can more easily observe the cellular and network mechanisms of learning while it happens than with in vivo models,

and ensure that any changes induced by the stimuli have functional consequences on hybrid behavior.

Acknowledgements

This work was partially supported by grants NS38628 from NIH/NINDS, and EB000786 from NIH/NIBIB, and by the Whitaker Foundation and the NSF Center for Behavioral Neuroscience. We thank Radhika Madhavan, Sheri McKinney and Eno Ekong for technical assistance.

References

- Bakkum, DJ.; Shkolnik, AC.; Ben-Ary, G.; Gamblen, P.; Demarse, TB.; Potter, SM. Removing some 'A' from AI: embodied cultured networks. In: Iida, F.; Steels, L.; Pfeifer, R., editors. *Embodied Artificial Intelligence*. Springer-Verlag; Berlin: 2004.
- Baruchi I, Ben-Jacob E. Functional holography of recorded neuronal networks activity. *J Neuroinformat* 2004;2:333–352.
- Beggs J, Plenz D. Neuronal avalanches are diverse and precise activity patterns that are stable for many hours in cortical slice cultures. *J Neurosci* 2004;24:5216–5229. [PubMed: 15175392]
- Bliss TV, Collingridge GLA. A synaptic model of memory: long-term potentiation in the hippocampus. *Nature* 1993;361:31–39. [PubMed: 8421494]
- Bliss TV, Lømo T. Long-lasting potentiation of synaptic transmission in the dentate area of the anaesthetized rabbit following stimulation of the perforant path. *J Physiol Lond* 1973;232:331–356. [PubMed: 4727084]
- Brooks, R. *Cambrian Intelligence, the Early History of the New AI*. The MIT press; Cambridge: 1999.
- Brown EN, Kass RE, Mitra PP. Multiple neural spike train data analysis: state-of-the-art and future challenges. *Nat Neurosci* 2004;7:456–461. [PubMed: 15114358]
- Caminiti R, Johnson PB, Burnod Y, Galli C, Ferraina S. Shifts of preferred directions of premotor cortical cells with arm movements performed across the workspace. *Exp Brain Res* 1990;83:228–232. [PubMed: 2073945]
- Davies DL, Bouldin DW. A cluster separation measure. *IEEE Trans Pattern Anal Machine Intell* 1979;1:224–227.
- DeMarse TB, Wagenaar DA, Blau AW, Potter SM. The neurally controlled animat: biological brains acting with simulated bodies. *Autonomous Robots* 2001;11:305–310. [PubMed: 18584059]
- Georgopoulos, AP. *Selectionism and the Brain*. Academic Press; San Diego: 1994. Population activity in the control of movement; p. 103-119.
- Gross GW, Kowalski JM. Origins of activity patterns in self-organizing neuronal networks in vitro. *J Intell Mat Sys and Struct* 1999;10:558–564.
- Gross, GW.; Rhoades, BK.; Kowalski, JK. Dynamics of burst patterns generated by monolayer networks in culture. In: Bothe, HW.; Samii, M.; Eckmiller, R., editors. *Neurobionics: An Interdisciplinary Approach to Substitute Impaired Functions of the Human Nervous System*. North-Holland; Amsterdam: 1993a. p. 89-121.
- Gross GW, Rhoades BK, Reust DL, Schwalm FU. Stimulation of monolayer networks in culture through thin-film indium-tin oxide recording electrodes. *J Neurosci Methods* 1993b;50:131–143. [PubMed: 8107494]
- Ikegaya Y, Aaron G, Cossart R, et al. Synfire chains and cortical songs: Temporal modules of cortical activity. *Science* 2004;304:559–564. [PubMed: 15105494]
- Izhikevich EM, Gally JA, Edelman GM. Spike-timing dynamics of neuronal groups. *Cereb Cortex* 2004;14:933–944. [PubMed: 15142958]
- Jimbo Y, Tateno T, Robinson HPC. Simultaneous induction of pathway-specific potentiation and depression in networks of cortical neurons. *Biophys J* 1999;76:670–678. [PubMed: 9929472]
- Kamioka H, Maeda E, Jimbo Y, Robinson HPC, Kawana A. Spontaneous periodic synchronized bursting during formation of mature patterns of connections in cortical cultures. *Neurosci Lett* 1996;206:109–112. [PubMed: 8710163]

- Kawaguchi H, Fukunishi K. Dendrite classification in rat hippocampal neurons according to signal propagation properties—observation by multichannel optical recording in cultured neuronal networks. *Exp Brain Res* 1998;122:378–392. [PubMed: 9827857]
- Krichmar J, Edelman G. Machine psychology: autonomous behavior, perceptual categorization and conditioning in a brain-based device. *Cereb Cortex* 2002;12:818–830. [PubMed: 12122030]
- Latham PE, Richmond BJ, Nirenberg S, Nelson PG. Intrinsic dynamics in neuronal networks. II. Experiment. *J Neurophys* 2000;83:828–835.
- Linden DJ. Long-term synaptic depression in the mammalian brain. *Neuron* 1994;12:457–472. [PubMed: 8155315]
- Madhavan, R.; Chao, ZC.; Potter, SM. Spontaneous bursts are better indicators of tetanus-induced plasticity than responses to probe stimuli. *Proc. 2nd Intl. IEEE EMBS Conf. On Neural Engineering*; 2005. p. 434-437.
- Madhavan, R.; Wagenaar, DA.; Chao, ZC.; Potter, SM. Control of bursting in dissociated cortical cultures on multi-electrode arrays. *Proc. Substrate-Integrated Micro-Electrode Arrays*; Denton, TX. 2003.
- Markram H, Gupta A, Uziel A, Wang Y, Tsodyks M. Information processing with frequency-dependent synaptic connections. *Neurobiology of Learning and Memory* 1998;70:101–112. [PubMed: 9753590]
- Marom S, Shahaf G. Development, learning and memory in large random networks of cortical neurons: Lessons beyond anatomy. *Quart Rev Biophys* 2002;35:63–87.
- McIntyre C, Grill W. Extracellular stimulation of central neurons: influence of stimulus waveform and frequency on neuronal output. *J Neurophys* 2002;88:1592–1604.
- Meyer, JA.; Wilson, SW. *From Animals to Animats: Proceedings of the First International Conference on Simulation of Adaptive Behavior*. MIT Press; Cambridge: 1991.
- Natschlagler, T.; Markram, H.; Maass, W. *A Practical Guide to Neuroscience Databases and Associated Tools*. 2002. Computer models and analysis tools for neural microcircuits.
- Pesaran B, Pezaris J, Sahani M, Mitra P, Andersen R. Temporal structure in neuronal activity during working memory in macaque parietal cortex. *Nat Neurosci* 2002;5:805–811. [PubMed: 12134152]
- Potter, SM. Two-photon microscopy for 4D imaging of living neurons. In: Yuste, R.; Konnerth, A., editors. *Imaging in Neuroscience and Development: A Laboratory Manual*. Cold Spring Harbor Laboratory Press; Cold Spring Harbor, NY: 2005. p. 59-70.
- Potter SM, DeMarse TB. A new approach to neural cell culture for long-term studies. *J Neurosci Methods* 2001;110:17–24. [PubMed: 11564520]
- Potter, SM.; Fraser, SE.; Pine, J. *Animat in a Petri Dish: Cultured Neural Networks for Studying Neural Computation*. Proceedings of the Fourth Joint Symposium on Neural Computation, UCSD; 1997. p. 167-174.
- Potter, SM.; Lukina, N.; Longmuir, KJ.; Wu, Y. Multi-site two-photon imaging of neurons on multi-electrode arrays. *SPIE Proc.*; 2001. p. 104-110.
- Potter, SM.; Wagenaar, DA.; DeMarse, TB. Closing the loop: stimulation feedback systems for embodied MEA cultures. In: Taketani, M.; Baudry, M., editors. *Advances in Network Electrophysiology Using Multi-Electrode Arrays*. Kluwer; New York: in press
- Rambani, K.; Booth, MC.; Brown, EA.; Raikov, I.; Potter, SM. Custom made multiphoton microscope for long-term imaging of neuronal cultures to explore structural and functional plasticity. *Proc. SPIE*; 2005. p. 102-108.
- Schaal, S.; Ijspeert, A.; Billard, A.; Vijayakumar, S.; Hallam, J.; Meyer, J., editors. *From animals to animats 8: Proceedings of the Eighth International Conference on the Simulation of Adaptive Behavior*. Bradford Books; Cambridge, MA: 2004.
- Segev R, Ben-Jacob E. Generic modeling of chemotactic based self-wiring of neural networks. *Neural Networks* 2000;13:185–199. [PubMed: 10935760]
- Shahaf G, Marom S. Learning in networks of cortical neurons. *J Neurosci* 2001;21:8782–8788. [PubMed: 11698590]
- Song S, Miller KD, Abbott LF. Competitive hebbian learning through spike-timing-dependent synaptic plasticity. *Nat Neurosci* 2000;3:919–926. [PubMed: 10966623]

- Tateno T, Jimbo Y. Activity-dependent enhancement in the reliability of correlated spike timings in cultured cortical neurons. *Biol Cybern* 1999;80:45–55. [PubMed: 9951397]
- Wagenaar DA, Madhavan R, Pine J, Potter S. Controlling Bursting in Cortical Cultures with Closed-Loop Multi-Electrode Stimulation. *J Neurosci* 2005;25:680–688. [PubMed: 15659605]
- Wagenaar, DA.; Madhavan, R.; Potter, SM. Stimulating news for MEA enthusiasts. SIMEA 2003; Denton, TX, USA. 2003.
- Wagenaar DA, Pine J, Potter S. Effective parameters for stimulation of dissociated cultures using multi-electrode arrays. *J Neurosci Methods* 2004;138:27–37. [PubMed: 15325108]
- Wagenaar DA, Potter SM. A versatile all-channel stimulator for electrode arrays, with real-time control. *J Neural Eng* 2004;1:39–45. [PubMed: 15876621]
- Wong ROL, Meister M, Shatz CJ. Transient period of correlated bursting activity during development of the mammalian retina. *Neuron* 1993;11:923–938. [PubMed: 8240814]

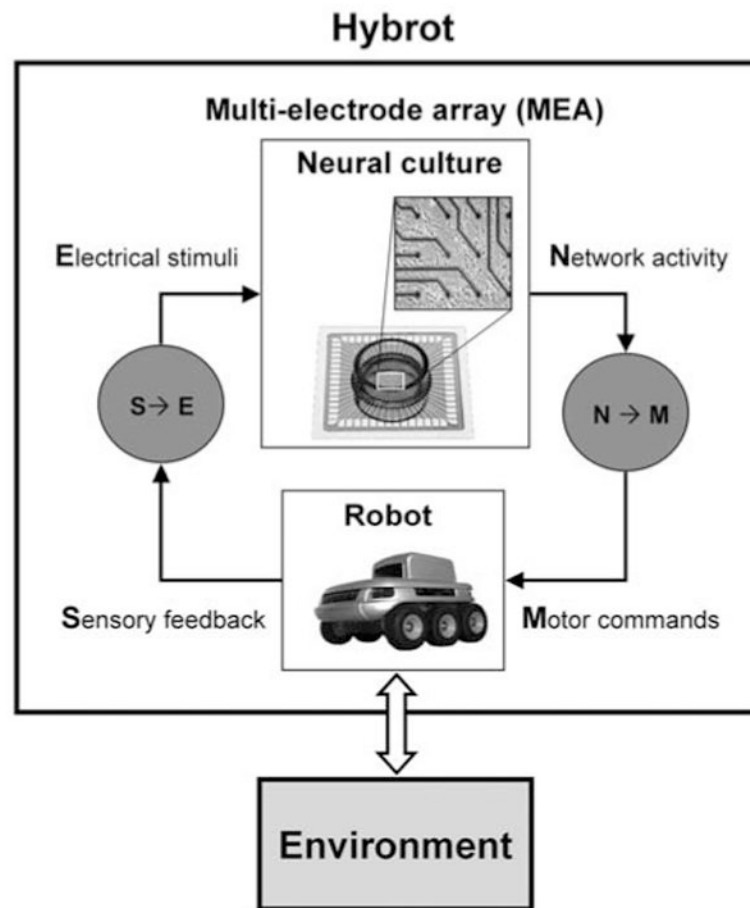


Fig. 1.

Hybrot, the embodied hybrid neural-robotic system: A hybrot consists of a cultured neuronal network, a robot, and a feedback loop. Network activity recorded from the cultured network is transferred into the robot's motor commands. This transfer function is the gray circle marked with "N→M." The interaction between the robot and its environment is detected by the robot's sensors and transferred into an electrical stimulation fed back to the cultured network. This transfer function is the gray circle marked with "S→E." The feedback affects the network activity and thus future motor commands. The MEA is capable of both recording and stimulating the cultured network at multiple locations simultaneously.

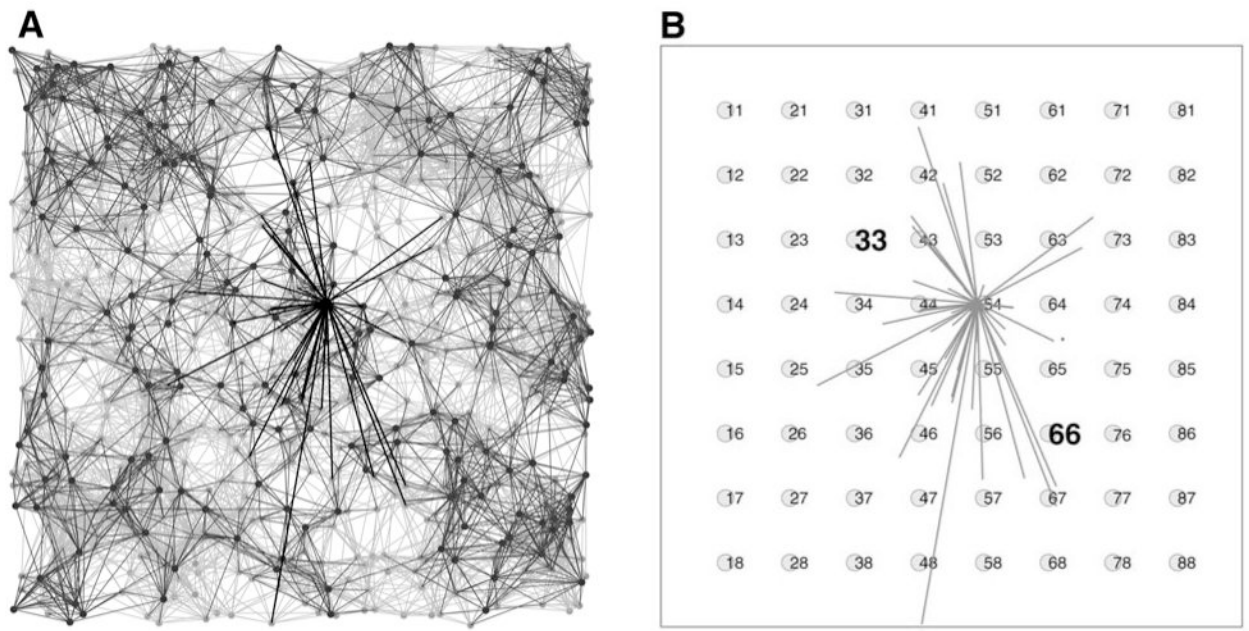
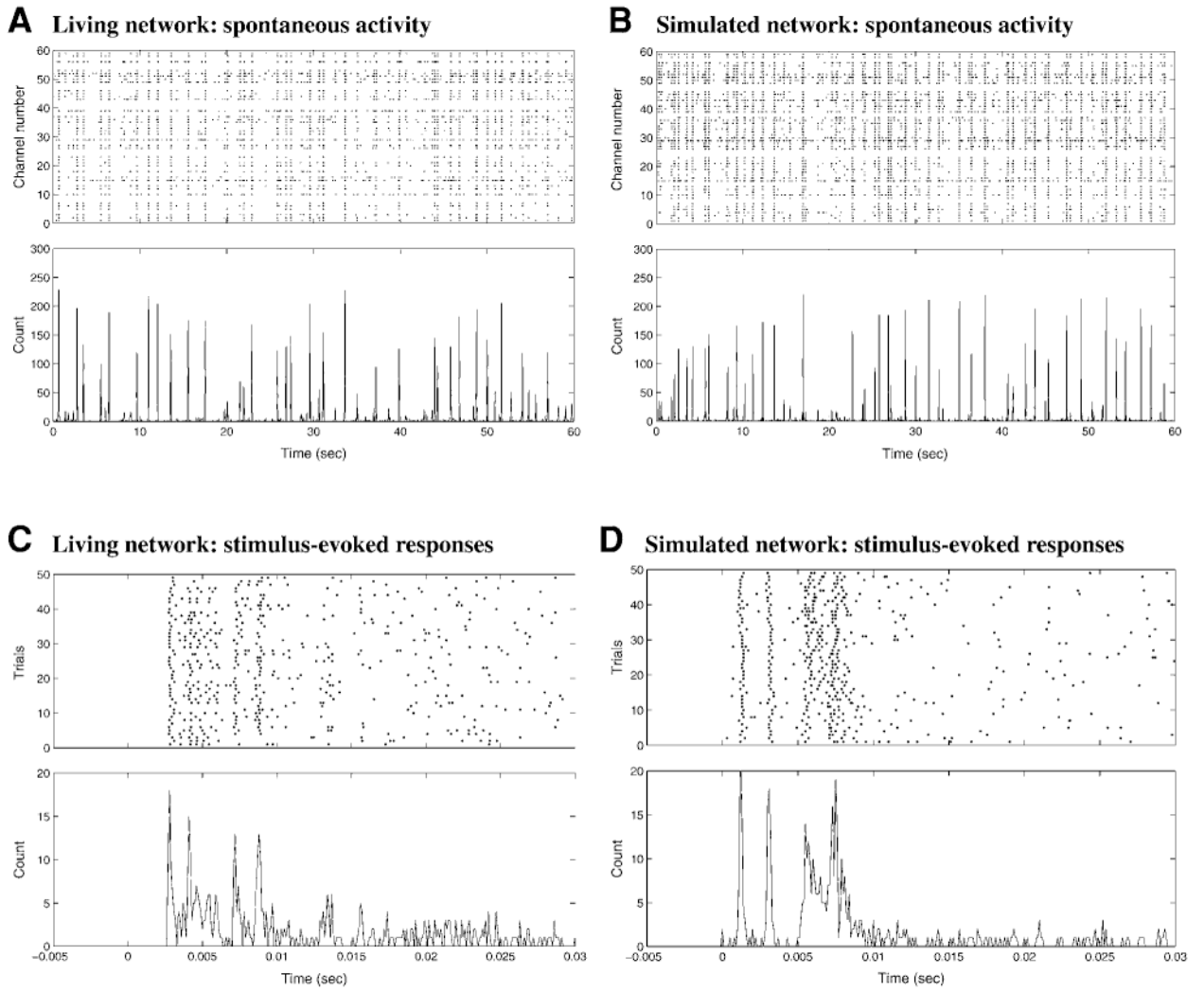


Fig. 2. Simulated network structure and positions of stimulation electrodes: Simulated neural network and stimulation electrodes were constructed to mimic the dissociated cultured network and MEA setup. **(A)** Structure of the simulated model network. One thousand LIF neurons are located in a $3\text{ mm} \times 3\text{ mm}$ region, the circles indicate the neurons, the light-gray lines represent the excitatory synapses and the dark-gray lines represent the inhibitory synapses. All neurons are shown but only 15% of the synaptic connections are shown for clarity. Thick black lines emphasize the connections from a particular randomly selected neuron. It had both long-range and local connections. **(B)** The locations of 64-electrodes are shown in circles, and marked with column-row numbers (tetanization channels 33 and 66 are emphasized). The connections of the neuron highlighted in (A) are depicted in light gray.

**Fig. 3.**

Comparison of the network activities from experimental data and simulation: Simulated spontaneous activity and evoked responses resemble the experimentally recorded data. One minute of spontaneous activity was recorded from a living network by a 60-channel MEA (**A**), and in simulation (**B**) for comparison. The upper panels are spike raster plots. The lower panels are firing rate histograms, with bin sizes of 100 ms. Also, 50 trials of evoked responses recorded by one electrode in a living network (**C**), and in simulation (**D**) are shown for comparison. The upper panels are spike raster plots. The lower panels are firing rate histograms, with the bin size of 0.1 ms. The timings of stimuli for each trial were aligned at time zero. In the simulation, each electrode recorded the activities occurring within 100 μm .

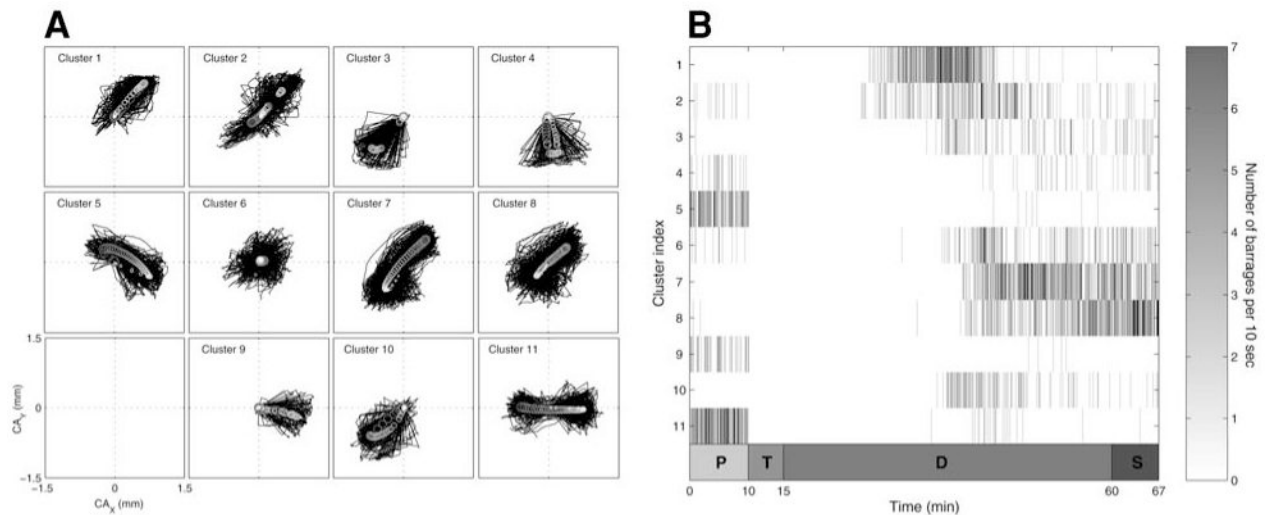
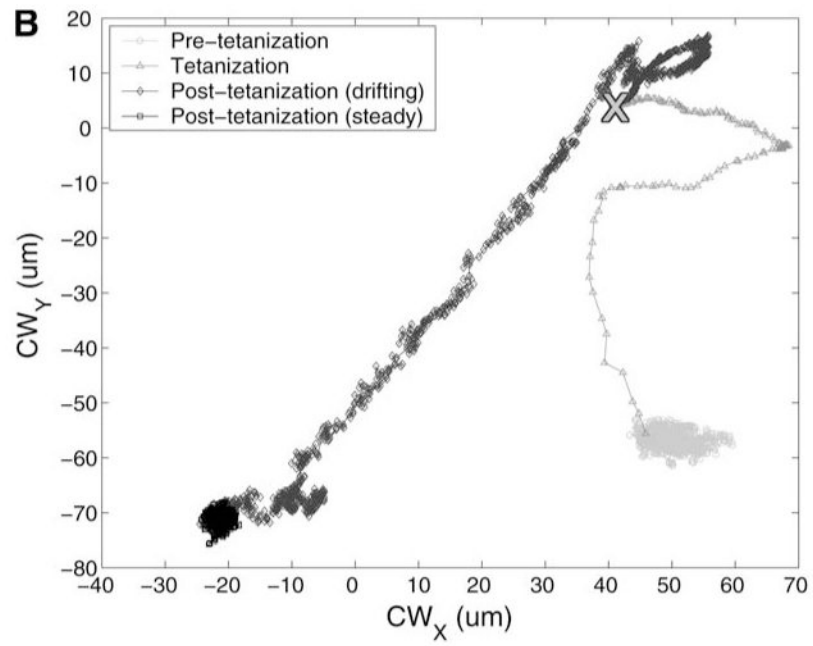
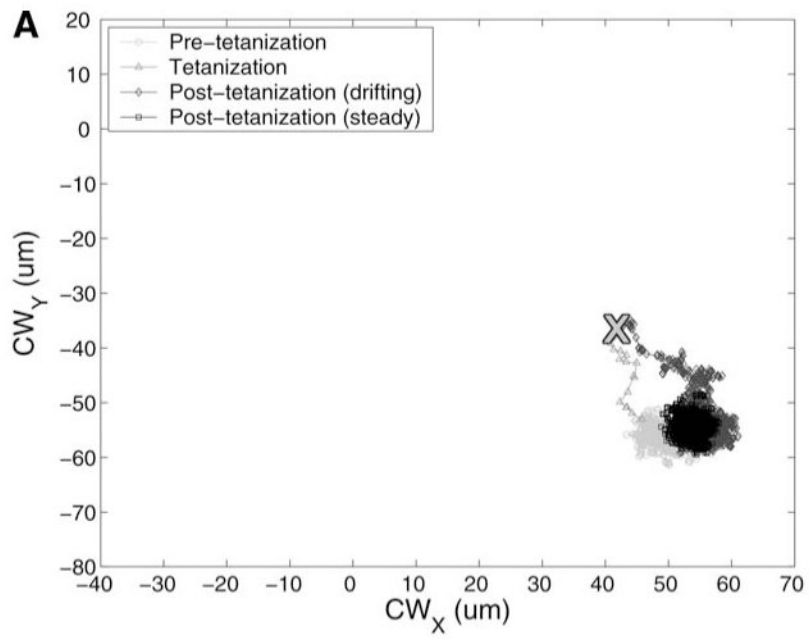


Fig. 4.

CA trajectory of spontaneous barrages in a “Long” experiment in one network: Different kinds of spontaneous barrages occurred in different periods. **(A)** Different classes of CA trajectories of spontaneous barrages. A total of 2387 barrages were detected. The CA trajectories of these barrages were classified by the *k*-means clustering algorithm, and eleven classes were found. The CA trajectories for different clusters were plotted separately. The coordinate shown in the lower-left corner represents the 3 mm × 3 mm area of the “dish”. The trajectories belonging to the same cluster are overlaid together. The averaged trajectories of each cluster are shown by a trace of circles, dark and large for the start of the trajectory, lighter and smaller toward the end. **(B)** The occurrences of different types of spontaneous barrages. The *x*-axis represents time in minutes, and the *y*-axis indicates the cluster index that corresponds to the index shown in (A). The shading represents the frequency of occurrences of the spontaneous barrages measured in every 10 s; the corresponding grayscale is shown at right. Notice that there is no spontaneous activity during tetanzation (from 10 to 15 min). Marked periods are: *P*, Pretetanzation; *T*, Tetanzation; *D*, Posttetanzation (drifting) and *S*, Posttetanzation (steady) (see Results and Fig. 5B).



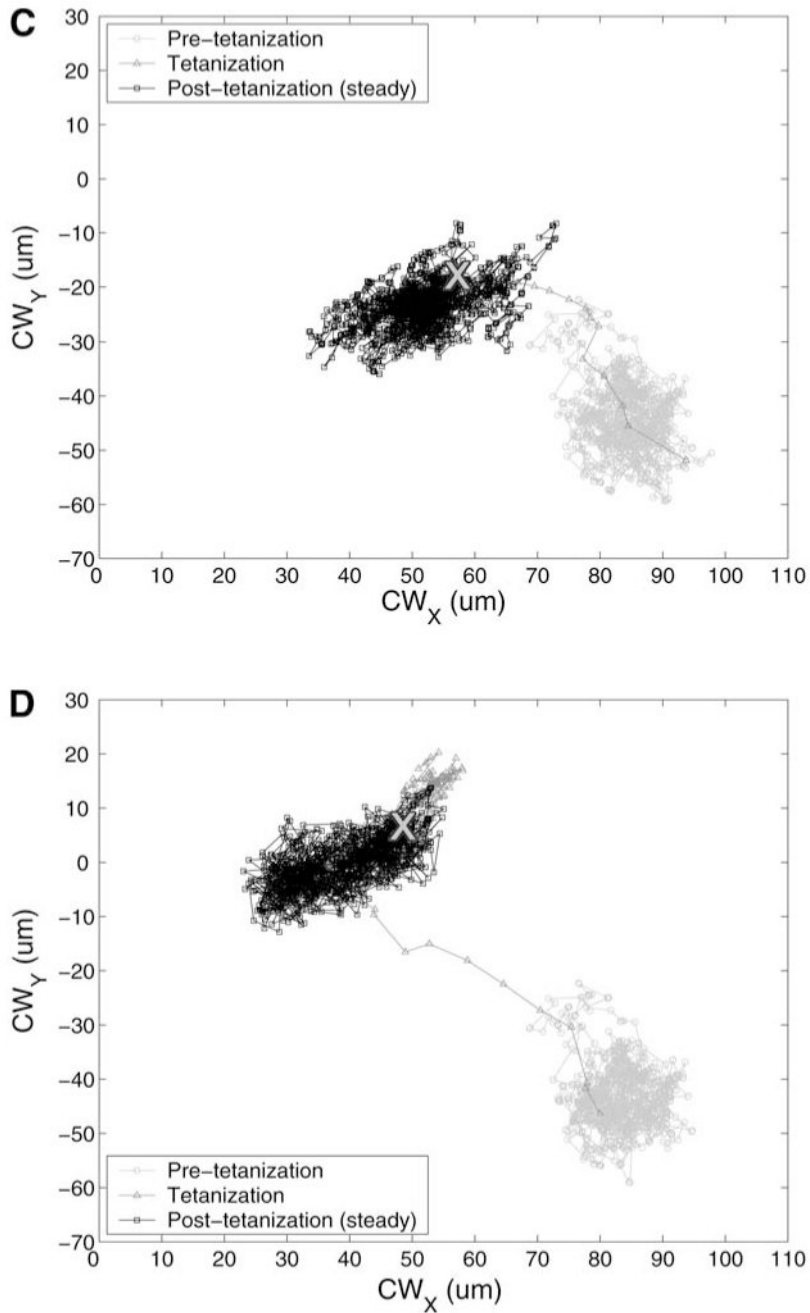
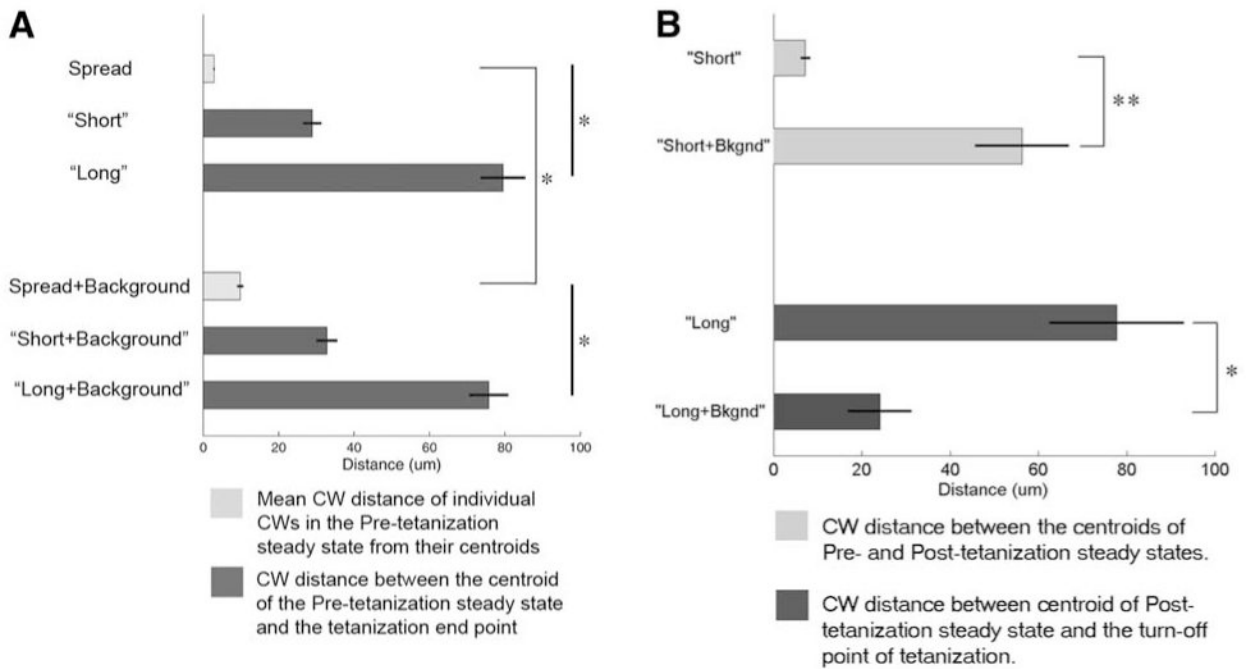


Fig. 5. Comparison of CW trajectories from four experimental conditions on each of five networks: Random multisite background stimulation maintained the network synaptic stability by reducing the “turning-back” and “drifting-away” of the CW trajectories after 10 s and 5 min tetanizations, respectively. CW trajectories, sampled at 2 Hz, are shown for one of the five networks for the “Short” experiment (**A**), the “Long” experiment (**B**), the “Short+Background” experiment (**C**) and the “Long+Background” experiment (**D**). The light-gray circles, mid-gray triangles, dark-gray diamonds, and black squares represent the pretetanzation period, tetanzation period, posttetanzation drifting period (in A and B only) and posttetanzation steady period, respectively. The turn-off points of tetanzation are marked with “X.” Notice

that with the random background stimulation, the CW trajectory stayed near the point where the short tetanization was turned off without turning back toward the pretetanization steady state (compare A and C). For long tetanizations, the random multisite background stimulation kept the CW trajectory near the point where the tetanization was turned off without drifting away (compare B and D).

**Fig. 6.**

Statistics of CW trajectories: Random background stimulation did not affect the amount of CW change induced by tetanzation, and had a stabilizing effect on CW trajectory after tetanzation. **(A)** The change of CW after tetanzation was significantly greater than the spread of CW in pretetanzation period. The spread of CW without background stimulation was significantly smaller than with background stimulation (marked, * $n = 5$ simulated networks, $p < 10^{-4}$). This spread was compared to the change of CW caused by tetanzation (*see Results*). Without background stimulation, the spread was significantly smaller than both the tetanzation-induced changes in the "Short" experiments ($p < 10^{-6}$) and the "Long" experiments ($p < 10^{-6}$). With background stimulation, the spread was significantly smaller than both the tetanzation-induced changes in the "Short+Background" experiments ($p < 10^{-4}$) and the "Long+Background" experiments ($p < 10^{-5}$). The CW change induced by long tetanzation was greater than that induced by short tetanzation, both without background stimulation ($p < 10^{-4}$) and with background stimulation ($p < 10^{-4}$). Vertical bars represent significant differences between values (marked, * $p < 10^{-4}$). **(B)** The CW distance between centroids of pre- and posttetanzation steady states was used to quantify "turning-back" of the CW trajectory after 10-s tetanzation (Fig. 5A). With random background stimulation, the CW of the Posttetanzation steady state stayed significantly farther from the pretetanzation steady state after the short tetanzation (marked, ** $p < 0.001$). The CW distance between the centroid of the posttetanzation steady state and the turn-off point of the tetanzation was used to quantify the "drifting-away" of the CW after the 5-min tetanzation (Fig. 5B). With random background stimulation, the CW of the posttetanzation steady state drifted significantly less after the long tetanzation than without (marked *, $p < 0.01$).

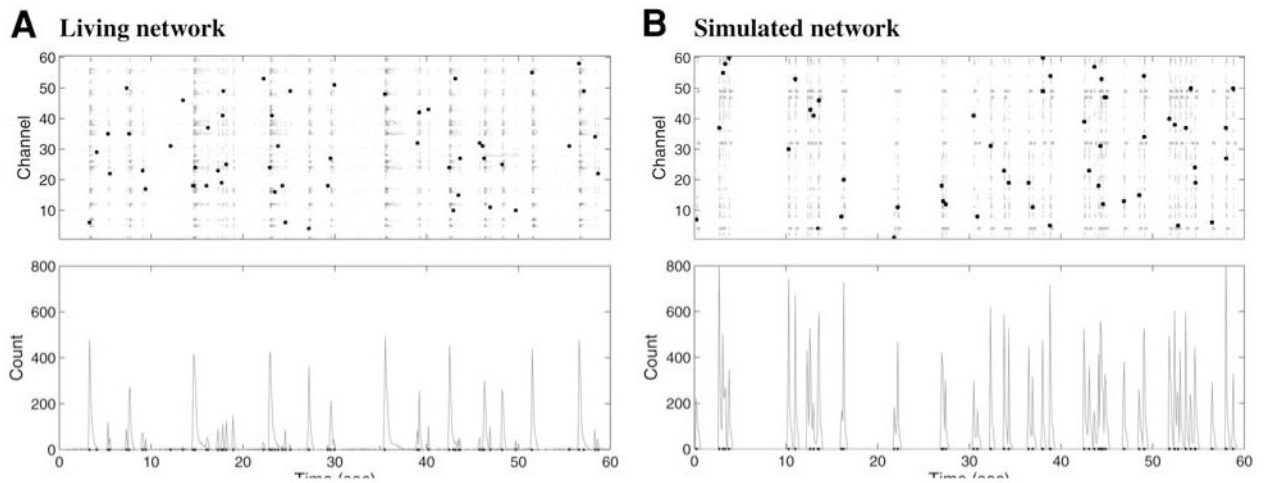


Fig. 7.

Comparison of network activity with random background stimulation in living and simulated networks: In the presence of background stimulation, the network activity consisted mostly of evoked responses, both in living networks and simulated networks. **(A)** A 1-min recording from a living network with background stimulation by 60-channel MEA is shown in a rasterplot (upper panel, spikes recorded in the i th electrode were randomly spread out in the interval $[i - 0.5 i + 0.5]$ on the y-axis for clarity) and the corresponding firing rate histogram (lower panel, bin size is 100 ms). **(B)** A 1-min simulation with background stimulation is shown as a raster plot (upper panel) and the corresponding firing rate histogram (lower panel). The timings and channels of applied stimuli are shown as black dots in the raster plots and on the x-axis in the histograms. The ratio of the number of evoked barrages vs spontaneous barrages was 41:1 in the living network compared to 42 : 3 in the simulated network. Moreover, the spontaneous barrage rate was reduced from 0.70 Hz (Fig. 3A) to 0.017 Hz (1 barrage in 1 min) in the living network and was reduced from 0.73 Hz (Fig. 3B) to 0.05 Hz (3 barrages in 1 min) in the simulated network.

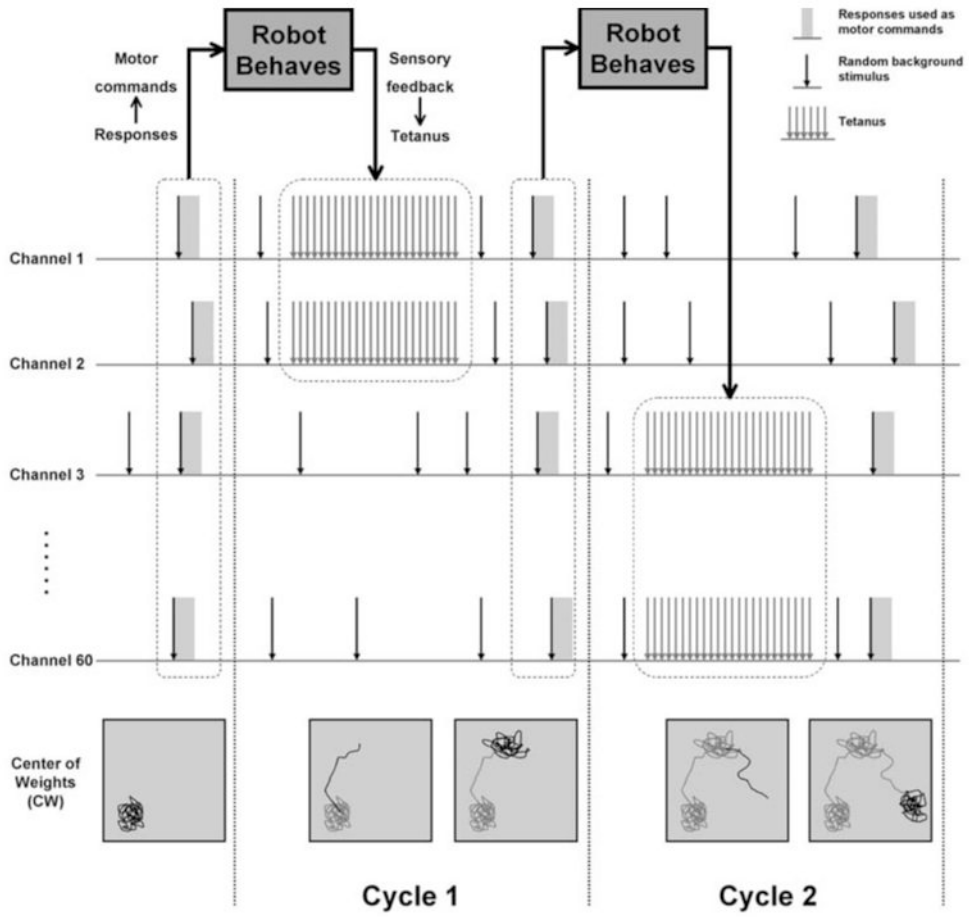


Fig. 8. A potential paradigm for hybrid control with random background stimulation and tetanization: Two and a half command cycles are depicted above, separated by vertical dotted lines. Each cycle consists of tetanus at two channels and continuous random background at all 60 channels. The CA trajectories of the responses to the most recent background stimulus at each channel in one cycle could be transformed into motor commands for a robot. The sensory feedback from the robot could be transformed into different forms of tetanization in the next cycle (in this figure, two different tetanizations are applied at two different pairs of electrodes). Based on our model, we expect the network synaptic weights to change in different ways depending on the sensory feedback since different tetanizations could have different effects. The continuous random background stimulation is expected to stabilize the weight changes (a series of hypothesized CW trajectories are shown in the bottom row). As a result, the behavior pattern of the hybrid would change after each sensory feedback and remain steady until the next feedback.